The FEBS Journal

FEBS PRESS science publishing by scientists

O_2-independent demethylation of trimethylamine *N*-oxide by Tdm of *Methylocella silvestris*

Yijun Zhu[1], Amira Z. Ksibe[2], Hendrik Schäfer[1], Claudia A. Blindauer[2], Timothy D. H. Bugg[2] and Yin Chen[1]

1 School of Life Sciences, University of Warwick, Coventry, UK
2 Department of Chemistry, University of Warwick, Coventry, UK

Keywords
crossover; DUF1989; non-haem iron; TMAO demethylase; zinc

Correspondence
Y. Chen, School of Life Sciences, University of Warwick, Coventry, CV4 7AL, UK
Fax: +44 24 76523568
Tel: +44 24 76528976
E-mail: Y.chen.25@warwick.ac.uk

(Received 22 July 2016, revised 9 September 2016, accepted 15 September 2016)

doi:10.1111/febs.13902

Bacterial trimethylamine *N*-oxide (TMAO) demethylase, Tdm, carries out an unusual oxygen-independent demethylation reaction, resulting in the formation of dimethylamine and formaldehyde. In this study, site-directed mutagenesis, homology modelling and metal analyses by inorganic mass spectrometry have been applied to gain insight into metal stoichiometry and underlying catalytic mechanism of Tdm of *Methylocella silvestris* BL2. Herein, we demonstrate that active Tdm has 1 molar equivalent of Zn^{2+} and 1 molar equivalent of non-haem Fe^{2+}. We further investigated Zn^{2+}- and Fe^{2+}-binding sites through homology modelling and site-directed mutagenesis and found that Zn^{2+} is coordinated by a 3-sulfur-1-O motif. An aspartate residue (D198) likely bridges Fe^{2+} and Zn^{2+} centres, either directly or indirectly via H-bonding through a neighbouring H_2O molecule. H276 contributes to Fe^{2+} binding, mutation of which results in an inactive enzyme, and the loss of iron, but not zinc. Site-directed mutagenesis of Tdm also led to the identification of three hydrophobic aromatic residues likely involved in substrate coordination (F259, Y305, W321), potentially through a cation–π interaction. Furthermore, a crossover experiment using a substrate analogue gave direct evidence that a trimethylamine-alike intermediate was produced during the Tdm catalytic cycle, suggesting TMAO has a dual role of being both a substrate and an oxygen donor for formaldehyde formation. Together, our results provide novel insight into the role of Zn^{2+} and Fe^{2+} in the catalysis of TMAO demethylation by this unique oxygen-independent enzyme.

Introduction

Bacterial trimethylamine *N*-oxide (TMAO) demethylase (Tdm) is a key enzyme involved in bacterial degradation of trimethylamine (TMA) and TMAO [1–3]. The enzyme was first proposed in the 1970s and has been partially purified from *Bacillus* sp. PM6 [4] and *Pseudomonas aminovorans* (now *Aminobacter aminovorans* [5]). Despite being purified from aerobic hosts, Tdm can convert TMAO anaerobically to equimolar amounts of dimethylamine (DMA) and formaldehyde (HCHO) (1 TMAO → 1 DMA + 1 HCHO) [2,3,5]. The gene encoding Tdm has only been identified very recently and it is now known that *tdm* is widely

Abbreviations
ADH, alcohol dehydrogenase; Asc, ascorbic acid; BS-DMA, benzenesulfonyl dimethylamine adduct; BS-MEA, benzenesulfonyl methylethylamine adduct; DMEA, dimethyethylamine; EDTA, ethylenediaminetetraacetic acid; GCV_T, glycine cleavage T protein; HCHO, formaldehyde; HMS, hydroxymethanesulfonate; ICP, inductively coupled plasma–mass spectrometry; MS, mass spectrometer; OES, optical emission spectrometer; Tdm, trimethylamine *N*-oxide demethylase; THF, tetrahydrofolate; TMAO, trimethylamine *N*-oxide.

distributed in nature, particularly in heterotrophic bacteria of the *Roseobacter* clade and the SAR11 clade in marine bacterioplankton [2].

Tdm is constituted of two domains, an uncharacterized DUF1989-containing domain at its N terminus and a tetrahydrofolate (THF)-binding domain (GCV_T) at its C-terminus. DUF1989 in Tdm shows modest sequence similarity (< 30%) to urea-carboxylase-associated proteins, whose functions in urea catabolism are as-yet unknown [6]. GCV_T domains, however, are found in several very well-characterized THF-dependent enzymes, such as glycine cleavage T protein [7] and dimethylsulfoniopropionate demethylase [8], with a function of binding THF to accept formaldehyde. Therefore, it has been proposed previously that the N-terminal DUF1989 domain of Tdm may play a role in substrate binding and subsequent catalysis, whereas its C-terminal GCV_T domain is responsible for HCHO conjugation with THF [3].

It has been suggested that metal ions may play a role in Tdm catalysis [4]. For example, the partially purified Tdm of *Bacillus* sp. PM6 was strongly activated by ferrous iron [4]. In agreement with the putative role of metals in catalysis, purified Tdm of *Methylocella silvestris* does not contain either flavin adenine dinucleotide (FAD) or nicotinamide adenine dinucleotide (NAD) [3]. Although a crystal structure for Tdm has yet to be solved, structures of three DUF1989-domain containing proteins (3ORU, 3SIY, 3DI4) available in the Protein Data Bank (PDB) database all contain zinc (Zn^{2+}). However, the types of metal(s) present in Tdm are yet to be established experimentally, and the metal stoichiometry is not known.

The aim of this study was therefore to determine the stoichiometry of the metal cofactors of Tdm in order to gain insight into the catalytic mechanism of oxygen-independent TMAO demethylation by this unusual bacterial Tdm.

Results

Tdm is a novel zinc-iron-dependent protein

Early studies in the 1970s have suggested that bacterial Tdm is a metal-dependent enzyme. The *Bacillus* Tdm is strongly stimulated by ferrous iron and reducing agents such as ascorbate and glutathione [3]. In agreement with these previous studies, we observed ~ 20% inhibition of Tdm activity when the purified enzyme was incubated with the metal chelator EDTA (Fig. 1A). To characterize the metal ion(s) in Tdm, we carried out ICP-MS metal scan analyses of purified recombinant Tdm from *Methylocella silvestris*, which detected the presence of Zn, Fe and Ni above background levels (data not shown).

To obtain a more accurate estimation of metal contents in Tdm, Zn, Fe, Ni as well as S (for accurate determination of protein concentrations) were quantified by ICP-OES. The results showed that 1 monomer of Tdm contained 0.97 ± 0.03 Zn^{2+} and 0.35 ± 0.02 iron in the as-isolated Tdm (CK-Tdm, Table 1). Trace amounts of Ni^{2+} (< 0.1 molar equivalents per Tdm monomer) were also found, potentially as a consequence of the Ni-IMAC purification step. To address whether Zn or Fe could be replaced by each other, Fe- and Zn-enriched Tdm (Fe-Tdm, Zn-Tdm) were purified from *E. coli* cultivated in media supplemented with either $Fe(NH_4)_2(SO_4)_2$ or $ZnCl_2$ (0.5 mM final concentration). Tdm expressed in Fe-supplemented media showed slightly, yet significantly, higher Fe^{2+} content (0.38 ± 0.02 mol per mol monomer) ($P < 0.05$), whereas Tdm expressed in Zn-supplemented media had reduced Fe^{2+} content (0.12 ± 0.01 mol per mol monomer), in coincidence with an increase of Zn^{2+} content (1.33 ± 0.03 mol per mol monomer) ($P < 0.05$), suggesting a replacement of Fe by Zn in purified Tdm. Additionally, Fe-enriched Tdm had a higher catalytic activity compared to that of CK-Tdm or Zn-enriched Tdm (Table 1). Purified Tdm had a K_m value ~ 4 mM, in line with that of the same enzyme purified from two other bacteria, *Pseudomonas aminovorans* (2 mM) and *Bacillus* sp. PM6 (2.85 mM) [4,5].

To further probe the iron species in as-isolated Tdm of *M. silvestris*, activity assays were performed with the addition of a reducing agent (ascorbic acid, Asc) or an oxidizing agent (hydrogen peroxide, H_2O_2) at varying concentrations. The results demonstrated that Tdm was sensitive to H_2O_2 and > 80% activity was lost upon incubation with 100 μM H_2O_2 (Fig. 1B), while Asc did not show any inhibition until a final concentration of 8 mM (Fig. 1B). Furthermore, when isolated Tdm was incubated with various divalent metal ions, it was observed that Fe^{2+} significantly enhanced Tdm activity, particularly in the presence of Asc (Fig. 1C). Interestingly, the activity of H_2O_2-pretreated Tdm can at least be partially restored by incubating with Asc and Fe^{2+} (Fig. 1D). Taken together, our data suggested a role of ferrous iron in the native as-isolated Tdm during catalysis.

Due to the traditional protein overexpression and purification procedures, oxygen-sensitive ferrous iron is prone to loss [9,10]. Our ICP-OES analyses of as-isolated Tdm may therefore have underestimated *in-vivo* iron contents in this protein (Table 1). To determine the optimal Fe^{2+} stoichiometry, a Fe^{2+} titration experiment was carried out. To eliminate the

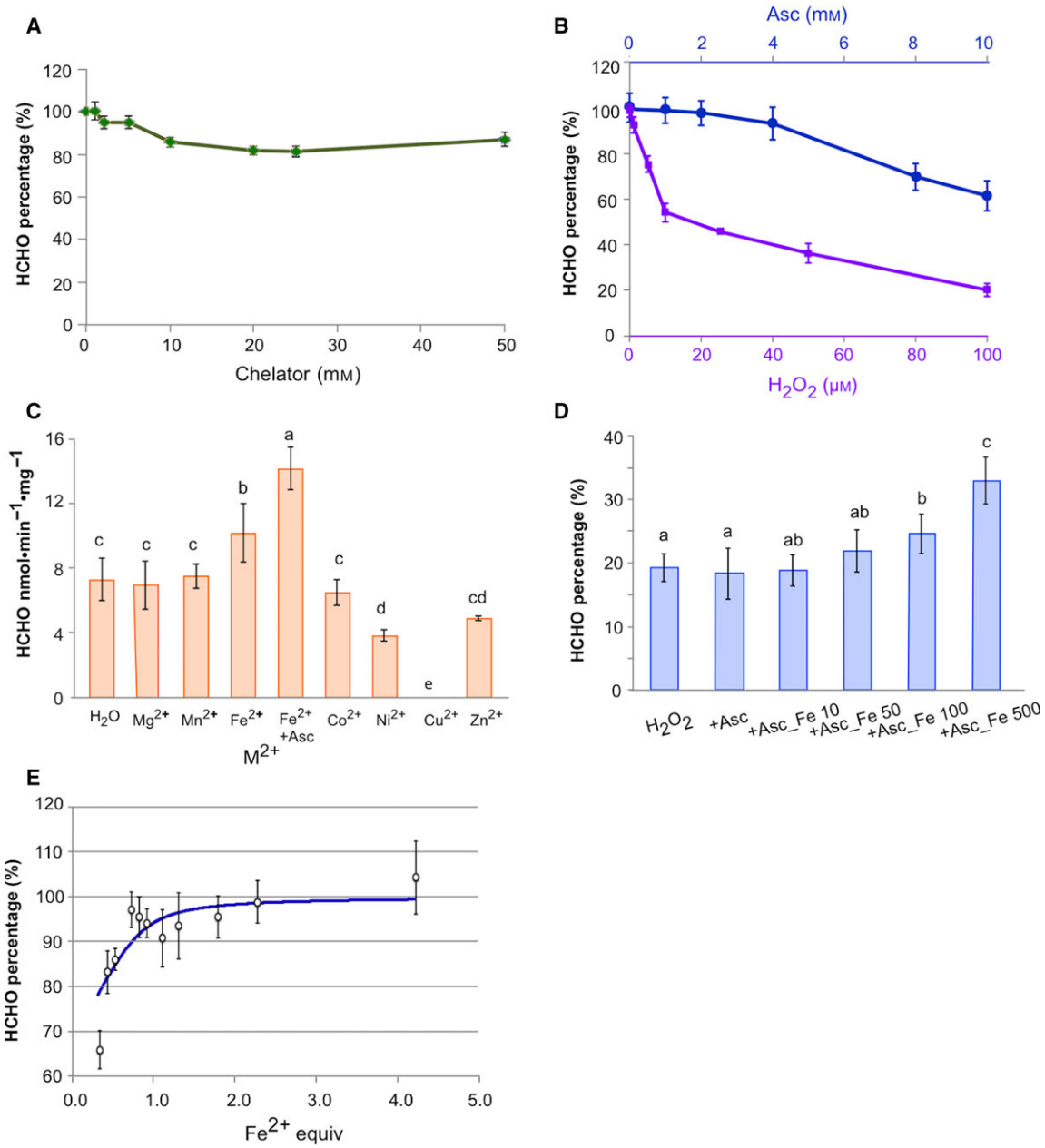

Fig. 1. Fe^{2+} is a native cofactor for Tdm. (A) Tdm activity was inhibited by EDTA. Error bars indicate SD of experiments run in triplicate. (B) The effects of H_2O_2 and ascorbic acid on Tdm activity. Tdm activity was measured by quantifying the formation of formaldehyde (HCHO). Blue: ascorbic acid; purple: H_2O_2. (C) The effects of additional metal ions on Tdm activity. The error bars represent SD from experiments run in triplicate. Different letters denote significant differences between different metal reconstitution ($P < 0.05$). Mg^{2+}: $MgCl_2$. Mn^{2+}: $MnCl_2$. Fe^{2+}: $Fe(NH_4)_2(SO_4)_2$. Co^{2+}: $CoCl_2$. Ni^{2+}: $NiSO_4$. Cu^{2+}: $CuSO_4$. Zn^{2+}: $ZnSO_4$. (D) The loss of Tdm activity by the addition of H_2O_2 can be partially restored by adding reducing agents in the enzyme assay. Tdm was pretreated with 100 μM H_2O_2 for 15 min. Inactivated Tdm was then reactivated by adding 500 μM ascorbic acid (Asc) and Fe^{2+} at varying concentration for 20 min before enzyme activity assay was carried out. H_2O_2: Tdm pretreated with 100 μM H_2O_2; +Asc: H_2O_2-pretreated Tdm incubated with 500 μM ascorbic acid; +Asc_Fe 10, +Asc_Fe 50, +Asc_Fe 100, +Asc_Fe 500: H_2O_2-pretreated Tdm incubated with 500 μM ascorbic acid and 10, 50, 100 or 500 μM of Fe $(NH_4)_2(SO_4)_2$ respectively. The error bars represent SD from experiments run in triplicate. Different letters denote significant differences between different metal reconstitution ($P < 0.05$). (E) Titration of as-isolated Tdm (Fe:Tdm ratio of 0.33 ± 0.02) with increasing concentrations of Fe^{2+} and the activity was measured by quantifying HCHO formation. Titration data were plotted using a nonlinear fitting using the multiple independent binding sites model [63,64], giving $n = 0.91$ per Tdm monomer. The error bars represent SD from experiments run in triplicate.

Table 1. Steady-state kinetic parameters of Zn- and Fe-enriched Tdm.

	CK-Tdm	Fe-Tdm	Zn-Tdm
K_m (mM)	3.88 ± 0.19[a]	4.09 ± 0.21[a]	4.29 ± 0.12[a]
V_{max} (nmol·min^{-1}·mg^{-1})	14.61 ± 1.13[a]	16.99 ± 0.70[b]	12.41 ± 0.52[c]
k_{cat} (s^{-1})	19.49 ± 1.51[a]	22.65 ± 0.94[b]	17.30 ± 1.37[c]
k_{cat}/K_m·M^{-1}·s^{-1} × 10^3	5.03 ± 0.34[a]	5.54 ± 0.36[a]	4.02 ± 0.22[b]
Metal equiv			
Zn^{2+}	0.97 ± 0.03[a]	0.92 ± 0.04[a]	1.33 ± 0.03[b]
Fe^{2+}	0.33 ± 0.02[a]	0.38 ± 0.02[b]	0.12 ± 0.01[c]

CK-Tdm, Tdm purified from recombinant *E. coli* cultivated using the LB medium; Fe-Tdm, the culture medium was supplemented with Fe $(NH_4)_2(SO_4)_2$ at a final concentration of 0.5 mM; Zn-Tdm, the culture medium was supplemented with $ZnCl_2$ at a final concentration of 0.5 mM. Values are means ± SD. Different superscript letters in the same row between samples denote significant differences between different metal enrichment ($P < 0.05$).

nonspecific binding of metal ions to the 6*His-tag, 6*His-tag-free Tdm was used. The data presented in Fig. 1E gave a stoichiometry number of $n = 0.91$. Together, our data suggest that Tdm is a Zn^{2+}- and Fe^{2+}-dependent protein with Zn^{2+}/Tdm and Fe^{2+}/Tdm monomer ratios of 1/1.

Three cysteine residues (C263, C279, C343) contribute to Zn^{2+} coordination in Tdm

The C-terminal GCV_T sequence is best characterized in the T protein of the glycine cleavage complex, which is required for glycine catabolism [7]. GCV_T has a THF-binding site for the conjugation of HCHO and this domain is not known to contain any metal cofactor. In agreement with the role of GCV_T domain in HCHO conjugation, we observed a significant reduction (~ 10%) of HCHO formation when additional THF was added to the enzyme assay. Similar observation has also been made in other enzymes that contain a GCV_T domain, such as the *N*-methylglutamate dehydrogenase in *Methyloversatilis universalis* FAM5 [11]. We thus postulate that metal-binding sites for Zn^{2+} and Fe^{2+} are likely located in the N-terminal uncharacterized DUF1989 domain.

The PDB database contains three entries for the DUF1989 protein family (3SIY, 3ORU, 3DI4), which all contain Zn^{2+} in their crystal structures. To predict the Zn^{2+}-binding sites in Tdm, homology modelling was therefore applied. The SWISS-MODEL template library was searched by profile-hidden Markov models (HMMs) HMM-HMM–based lightning-fast iterative sequence search (HHblits). Both algorithms indicated that the N-terminal domain of Tdm (residues 128–352) gave the highest sequence identity (34%) to the sequence of a protein of unknown function 3ORU (1.1 Å), which was therefore chosen as the reference structure for modelling.

The established model predicted a conserved Zn^{2+} coordination motif in *M. silvestris* Tdm, despite its poor global and per-residue model quality, assessed using the QMEAN scoring function (Qualitative Model Energy Analysis) [12]. In agreement with the existing structures of DUF1989 family proteins in the PDB database, homology modelling predicted that Zn^{2+} was coordinated by three cysteine residues in Tdm (Cys263, Cys279, Cys343) with the thiol S-Zn^{2+} distance around 2.3 Å (Fig. 2A). Multiple sequence alignment of Tdm proteins from a range of microbes of terrestrial and oceanic origins covering α-, β- and

Fig. 2. Determination of Zn^{2+}, Fe^{2+} and potential substrate-binding site in Tdm. (A) Homology modelling of the DUF1989 domain in Tdm (blue) suggests that C263, C279 and C343 are potential Zn^{2+}-binding sites. The existing structure of a DUF1989 family protein (3ORU, Magenta) was chosen as the template. (B) Superimposition of Zn^{2+}-binding motif of 3ORU (magenta) with catalytic Zn^{2+} site of cytidine deaminase (CDA) of *Mycobacterium tuberculosis* (3IJF, blue) and *Aspergillus terreus* (2Z3G, golden). Zn^{2+} ion is shown as grey sphere. Water is shown as red sphere. (C, D) D198 and H279 are Fe^{2+}-binding sites in Tdm. D198 is likely involved in Zn^{2+} coordination either indirectly through H-bonding with Zn^{2+}-bound water (C) or directly to Zn^{2+} ion (D). (E) Multiple sequence alignment of bacterial Tdm proteins (Uniprot accession numbers are shown) and two DUF1989 family protein entries whose structures are available from the PDB database (Q5LXE3; Q1GJV4). B8EIZ6: *Methylocella silvestris* BL2; C3K8G9: *Pseudomonas fluorescens* SBW25; Q5LT52: *Ruegeria pomeroyi* DSS-3; Q986L6: *Mesorhizobium loti* MAFF303099; F5RCR6: *Methyloversatilis universalis* FAM5; B6BQC7: *Candidatus* Pelagibacter sp. HTCC7211; J9Z2K4: *alphaproteobacterium* strain HIMB59. The conserved putative Zn^{2+} (C263, C279, C343) and Fe^{2+} (H256 and H276) coordination centres are highlighted in red boxes. Conserved aromatic amino acid residues in Tdm but not Q5LXE3 or Q1GJV4 are indicated by asterisk (*). Potential residues contributing to the formation of the substrate pocket (F259, Y305, W321) are indicated by arrows. (F) Far-UV CD spectra of wild-type Tdm (WT) and site-directed protein variants (C263, C279, C343, H256, H276, D198, F259, Y305, W321).

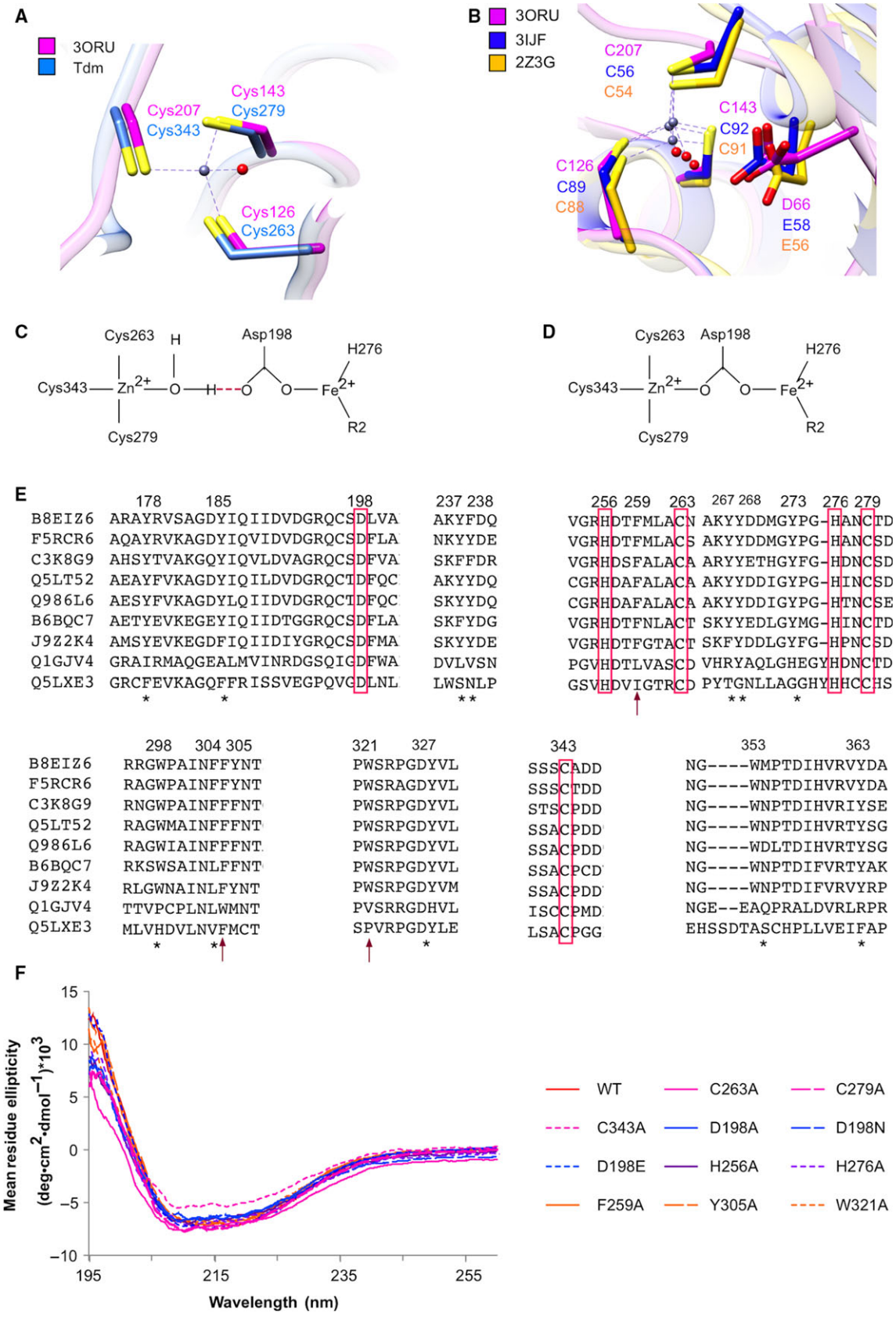
A
3ORU
Tdm
Cys207
Cys343
Cys143
Cys279
Cys126
Cys263
B
3ORU
3IJF
2Z3G
C207
C56
C54
C143
C92
C91
C126
C89
C88
D66
E58
E56
C
Cys263
H
Asp198
H276
Cys343
Zn2+
O
H
O
O
Fe2+
Cys279
R2
D
Cys263
Asp198
H276
Cys343
Zn2+
O
O
Fe2+
Cys279
R2
E
178 185 198 237 238
B8EIZ6 ARAYRVSAGDYIQIIDVDGRQCSDLVA AKYFDQ
F5RCR6 AQAYRVKAGDYIQVIDVDGRQCSDFLA NKYYDE
C3K8G9 AHSYTVAKGQYIQVLDVAGRQCSDFVA SKFFDR
Q5LT52 AEAYFVKAGDYIQILDVDGRQCTDFQC AKYYDQ
Q986L6 AESYFVKAGDYLQIIDVDGRQCTDFQC SKYYDQ
B6BQC7 AETYEVKEGEYIQIIDTGGRQCSDFLA SKFYDG
J9Z2K4 AMSYEVKEGDFIQIIDIYGRQCSDFMA SKYYDE
Q1GJV4 GRAIRMAQGEALMVINRDGSQIGDFWA DVLVSN
Q5LXE3 GRCFEVKAGQFFRISSVEGPQVGDLNL LWSNLP
256 259 263 267 268 273 276 279
B8EIZ6 VGRHDTFMLACN AKYYDDMGYPG-HANCTD
F5RCR6 VGRHDTFMLACS AKYYDDMGYPG-HANCSD
C3K8G9 VGRHDSFALACA ARYYETHGYFG-HDNCSD
Q5LT52 CGRHDAFALACA AKYYDDIGYPG-HINCSD
Q986L6 CGRHDAFALACA AKYYDDIGYPG-HTNCSE
B6BQC7 VGRHDTFNLACT SKYYEDLGYMG-HINCTD
J9Z2K4 VGRHDTFGTACT SKFYDDLGYFG-HPNCSD
Q1GJV4 PGVHDTLVASCD VHRYAQLGHEGYHDNCTD
Q5LXE3 GSVHDVIGTRCD PYTGNLLAGGHYHHCCHS
298 304 305 321 327
B8EIZ6 RRGWPAINFFYNT PWSRPGDYVL
F5RCR6 RAGWPAINFFYNT PWSRAGDYVL
C3K8G9 RNGWPAINFFFNT PWSRPGDYVL
Q5LT52 RAGWMAINFFFNT PWSRPGDYVL
Q986L6 RAGWIAINFFFNT PWSRPGDYVL
B6BQC7 RKSWSAINLFFNT PWSRPGDYVL
J9Z2K4 RLGWNAINLFYNT PWSRPGDYVM
Q1GJV4 TTVPCPLNLWMNT PVSRRGDHVL
Q5LXE3 MLVHDVLNVFMCT SPVRPGDYLE
343 353 363
SSSCADD NG----WMPTDIHVRVYDA
SSSCTDD NG----WNPTDIHVRVYDA
STSCPDD NG----WNPTDIHVRIYSE
SSACPDD NG----WNPTDIHVRTYSG
SSACPDD NG----WDLTDIHVRTYSG
SSACPCD NG----WNPTDIFVRTYAK
SSACPDD NG----WNPTDIFVRVYRP
ISCCPMD NGE--EAQPRALDVRLRPR
LSACPGG EHSSDTASCHPLLVEIFAP
F
Mean residue ellipticity (deg·cm2·dmol−1)×10^3
15
10
5
0
−5
−10
195
215
235
255
Wavelength (nm)
WT
C263A
C279A
C343A
D198A
D198N
D198E
H256A
H276A
F259A
Y305A
W321A

Table 2. Activity and metal quantification of wild-type Tdm and variants.

	Oligomeric status	Activity ($nmol \cdot min^{-1} \cdot mg^{-1}$)	M^{2+}/Tdm ratio	
			Zn^{2+}	Fe^{2+}
WT	Hexamer	14.61 ± 1.13	0.97 ± 0.03[a]	0.33 ± 0.02[a]
C263A	Monomer	0	0.44 ± 0.01[g]	0.04 ± 0.05[de]
C279A	Monomer	0	0.26 ± 0.14[h]	0.03 ± 0.01[e]
C343A	Aggregate/monomer	0	0.23 ± 0.09[h]	0.04 ± 0.03[de]
D198A	Unknown	0	0.66 ± 0.05[e]	0.12 ± 0.01[c]
D198N	Aggregate/hexamer	0	0.67 ± 0.02[e]	0.18 ± 0.02[b]
D198E	Aggregate/hexamer	0	0.53 ± 0.01[f]	0.33 ± 0.01[a]
H256A	Monomer	0	0.72 ± 0.01[d]	0.04 ± 0.01[e]
H276A	Hexamer	0	0.91 ± 0.01[b]	0.09 ± 0.02[d]
F259A	Hexamer	0	0.87 ± 0.03[c]	0.05 ± 0.00[e]
W321A	Hexamer	0	0.83 ± 0.03[c]	0.11 ± 0.00[c]
Y305A	Hexamer	0	0.94 ± 0.03[a]	0.15 ± 0.02[b]

Values are means ± SD. Different superscript letters in the same column between samples denote significant differences between different metal reconstitution ($P < 0.05$).

γ-proteobacteria revealed strict conservation of this 3-Cys Zn^{2+}-binding motif in Tdm (Fig. 2E).

To probe the role of these residues in Tdm activity, site-directed protein variants were constructed. These variants were purified and their activities and metal contents were characterized. The results showed that all three single variants were inactive, along with significantly reduced Zn^{2+} and Fe^{2+} contents ($P < 0.05$) (Table 2). Although CD spectroscopy revealed only very minor changes in overall secondary structure of these three variants (Fig. 2F), the native homohexamer, which dominates in wild-type Tdm, was virtually absent in the variants (Table 2). Together, the results suggested that C263, C279 and C343 are crucial for maintaining structural integrity, and as a consequence enzymatic activity, in native Tdm.

H276 is a potential Fe^{2+}-binding ligand in Tdm

Due to the lack of a crystal structure of Tdm and the absence of Fe^{2+} in existing crystal structures of DUF1989 family proteins, we performed multiple sequence alignment of Tdm sequences in order to gain insight into conserved residues, which may shed light on the residues involved in Fe^{2+} coordination (Fig. 2E). A 2-His-1-carboxylate facial triad is a common motif in a number of non-haem Fe^{2+}-containing enzymes, where two histidine residues and one carboxylate-containing side chain are arranged at one face of an octahedron, whereas the opposite face of the octahedron is available to coordinate a variety of exogenous ligands [13,14]. Our sequence alignment revealed the presence of two strictly conserved histidines (H256, H276) in all Tdm sequences analysed (Fig. 2E).

In order to test whether H256 and H276 were indeed Fe^{2+}-binding sites, point mutation variants were constructed, and the variants were subsequently purified and characterized. Data presented in Table 2 revealed that the two variants (H256A, H276A) were completely inactive. Metal analysis showed that the H276A variant indeed had lost Fe^{2+}, but its Zn^{2+} content remained unchanged compared to that of the wild-type Tdm. Furthermore, the loss of Fe^{2+} in the H276A variant cannot be attributed to a structural alteration caused by site-directed mutagenesis as its secondary and quaternary structure is comparable to that of the wild-type (Fig. 2F, Table 2).

The H256A variant was also inactive and had almost completely lost its Fe^{2+}. It also had a significantly lower Zn^{2+} content (Zn^{2+}/Tdm monomer ratio was 0.72 ± 0.01, compared to 0.97 ± 0.03 for wild-type) (Table 2). Although its secondary structure remained largely unchanged as revealed by CD spectroscopy, this variant did not form the native hexamer (Table 2). Therefore, H256 likely also plays a role in maintaining overall structure.

The 'bridging' nature of D198 in Tdm

The three existing crystal structures of DUF1989 family proteins (i.e. 3ORU) employ a 3-Cys-OH_2 Zn^{2+}-binding motif with the fourth ligand being a water molecule in the crystal structure (Fig. 2B). Searching the immediately surrounding zone (< 2.5 Å) [15,16] of the Zn^{2+} ion did not reveal any other potential ligands.

Although cysteines are commonly found in structural Zn sites, the 3-Cys-OH_2 tetrahedral coordination motif is found in the catalytic sites of several enzymes, e.g. cytidine deaminase (CDA) from *Mycobacterium tuberculosis* (3IJF) [17], man (1MQ0) [18] and mouse (1ZAB) [19], and the CDA-related enzyme, Blasticidin S deaminase, from *Aspergillus terreus* (2Z3G, 1WN6) [20]. In these structures, the catalytic H_2O forms a H-bond to a carboxylate oxygen of a glutamate and the main chain nitrogen of a Cys in the vicinity. In these enzymes, the zinc ion appears to act as electrophilic catalyst through this accompanying water molecule. Structure superimposition revealed that the 3-Cys-OH_2 motif of 3ORU is similar to CDA (Fig. 2B). D66 of 3ORU is in a similar position as the conserved Glu in CDA, i.e. E58 of 3IJF and E56 of 2Z3G (Fig. 2B), indicating that D66 may also H-bond to the Zn^{2+}-bound H_2O (Fig. 2C).

Multiple sequence alignment of various Tdm proteins and DUF1989 family proteins demonstrated strict conservation of this aspartate residue (corresponding to D198) in Tdm (Fig. 2E). To investigate whether D198 has any significance for TMAO demethylation by Tdm, three site-directed variants were made, D198A (no oxygen atom), D198N (one oxygen atom, neutral side chain) and D198E (two oxygen atoms, negatively charged). All three variants were inactive, and their Zn^{2+} contents (Zn^{2+}/Tdm ratios between 0.5 and 0.7) were significantly lower than that of the WT (0.97 ± 0.03) ($P < 0.05$) (Table 2). Although their overall secondary structure remained largely unchanged, alteration of quaternary structure was observed and the variants were prone to aggregation (Fig. 2F, Table 2).

The Fe^{2+} content of D198 variants varied considerably, following the trend of D198A (0.12 ± 0.01) < D198N (0.18 ± 0.02) < D198E (0.33 ± 0.01). Of the three D198 variants analysed, only the D198E variant retained its binding capacity for Fe^{2+}, similar to that of the wild-type Tdm (0.33 ± 0.02). It also retained hexameric state as observed in the wild-type enzyme (Table 2). Therefore, our data suggest that D198 also likely provides a carboxyl group for Fe^{2+} binding.

The substrate-binding pocket

TMAO-binding pockets have been studied previously in two enzymes, namely the substrate-binding protein (TmoX) of the TMAO ABC transporter and TMAO reductase (TorT) [21,22]. In both proteins, a hydrophobic substrate-binding pocket, composed of three to four aromatic residues, was found to recognize and bind TMAO via cation–π interaction [23]. Sequence alignment of Tdm proteins indeed revealed the presence of several conserved phenylalanine (Phe), tyrosine (Tyr) and tryptophan (Trp) residues (Fig. 2E). In an attempt to identify TMAO-binding sites in Tdm, we generated site-directed variants by individually replacing these Phe, Tyr and Trp residues with Ala. Three of these variants, F259A, Y305A and W321A, had completely lost activity (Table 2), while the overall secondary and quaternary structure was retained (Fig. 2F, Table 2), suggesting a role of these aromatic residues in substrate binding. Substitution of F259, Y305 and W321 with Ala may have changed hydrophobicity of adjacent Fe^{2+} centre and lead to significantly less Fe^{2+} content than WT (Fe^{2+}/Tdm ratios between 0.05 and 0.15) ($P < 0.05$). The remainder of the variants (Y185A, Y237A, Y267A, Y273A, W298A, W327A, Y363A) were, however, still active, thus these residues are unlikely to contribute to substrate binding.

The catalytic mechanism of TMAO degradation by Tdm

TMAO degradation catalysed by Tdm resembles *N*-dealkylation by other non-haem Fe^{2+}-containing enzymes, such as DNA dealkylase (AlkB) [24], histone demethylase (JHDM1, JMJD6) [25,26] and Rieske-type demethylase [27,28]. A high-valent Fe(IV)-oxo complex is a common active species for attacking the C-H bond of saturated carbon centres by non-haem Fe^{2+}-containing proteins. O_2 is required as oxygen donor for all the aforementioned reactions to form the Fe(IV)-oxo complex. However, a previous study on bacterial Tdm suggested that TMAO demethylation is O_2-independent [5]. Our enzyme assays performed using purified Tdm showed no difference in kinetics between aerobically and anaerobically conducted reactions, supporting that TMAO demethylation is indeed O_2-independent (Fig. 3A). The O_2-independency therefore suggests that TMAO may function as both the substrate and the oxygen donor for the subsequent demethylation. Although such a mechanism of surrogate oxygen donation has not been observed in non-haem iron enzymes, it has been found in haem-containing P450 enzymes in the absence of NAD(P)H and oxygen (reviewed in ref. [29,30]). Based on the well-studied P450 enzymes, we propose a putative Tdm catalytic cycle (Fig. 3B), where a high-valent oxidant (e.g. Fe(IV)-oxo) is generated through oxygen atom transfer from TMAO and a tertiary amine intermediate (i.e. trimethylamine, TMA) is formed, which then serves as a substrate for oxidative demethylation to DMA.

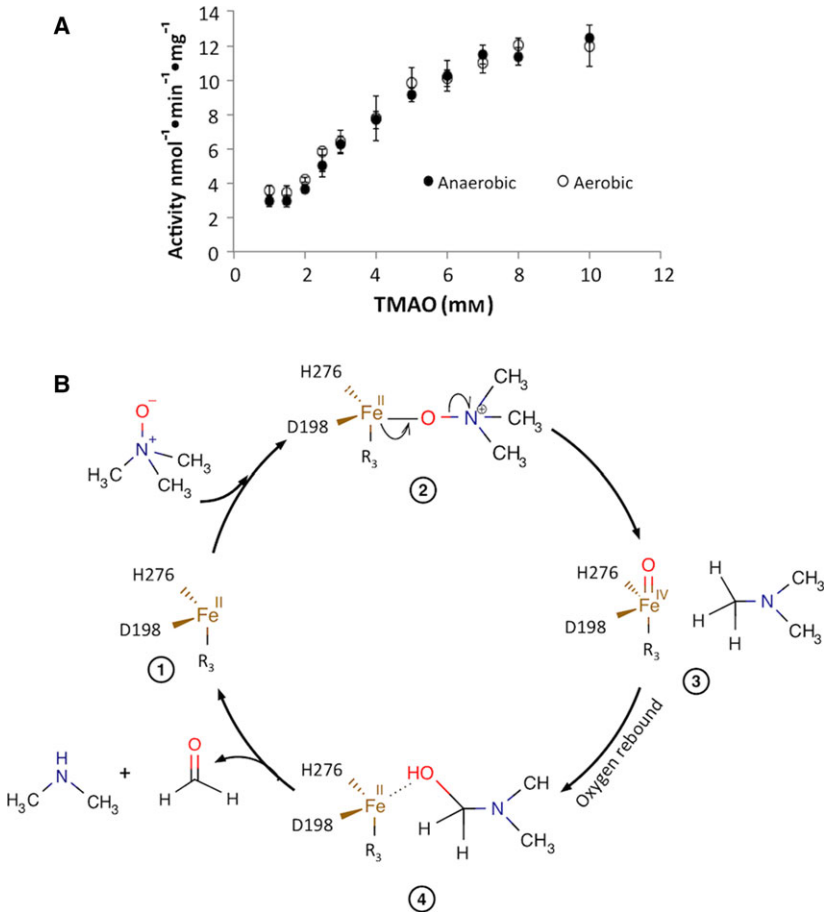

Fig. 3. Proposed mechanism of Tdm. (A) Tdm catalyses an O_2-independent demethylation of TMAO. The error bars represent SD from experiments run in triplicate. (B) Schematic diagram of the proposed mechanism of Tdm catalytic cycle. The substrate is proposed to act as the oxygen donor to activate the Fe centre ② to form a putative high-valent iron-oxo intermediate (e.g. Fe(IV)-oxo) ③, which then hydroxylates the N-methyl group to give an intermediate ④ that decomposes in water to form dimethylamine (DMA) and formaldehyde (HCHO). Meanwhile, Tdm returns to its ferrous resting state ①.

To test this hypothesis, we performed a crossover experiment using a TMA analogue in order to trap the formation of putative secondary amine species that can be released during the Tdm catalytic cycle [31]. *N, N*-dimethylethylamine (DMEA), a structural analogue of the postulated TMA intermediate, was added to the enzyme assays with and without the substrate, TMAO. If the tertiary amine intermediate (TMA) is formed and acts as a substrate during the catalytic cycle, a postulated high-valent Fe species, e.g. Fe(IV)-oxo, may also demethylate its analogue DMEA, hence forming the corresponding secondary amine species, methylethylamine (MEA) (Fig. 4A). The secondary amine products (DMA, MEA) were derivatized by benzenesulfonyl chloride (BSC) and quantified by GC-MS. In the absence of TMAO, Tdm does not catalyse the demethylation of DMEA. However, in the presence of TMAO, both DMA (*m/z*: 77.1, 141.1, 185.1) and MEA (*m/z*: 77.1, 141.1, 184.1) were detected, and DMA formation was competitively reduced in the presence of DMEA (Fig. 4B–D). The results therefore supported the postulated mechanism, confirming that TMAO is required as the oxygen donor, and that the resulting tertiary amine is a substrate for oxidative demethylation during the catalytic cycle of Tdm.

Discussion

Tdm is a novel Zn^{2+}- and Fe^{2+}-containing metalloprotein

In this report, we presented data suggesting that Tdm is a Zn^{2+}- and Fe^{2+}-dependent metalloenzyme and the $Zn^{2+}/Fe^{2+}/$Tdm monomer ratio is likely to be 1/1/1. It is noteworthy that both Zn^{2+} and Fe^{2+} are in the close vicinity of D198. Therefore, it is possible that Tdm has a cocatalytic binuclear Zn^{2+}–Fe^{2+} centre. Binuclear Zn/Fe sites have been found in many enzymes throughout nature, such as glycerophosphodiesterase [32], glyoxalase II [33], enamidase [34] and protein phosphatase 2B [35]. However, unlike Tdm, in these binuclear Zn/Fe hydrolases, Zn^{2+} is predominantly coordinated by histidine side chains.

Our data suggest that in Tdm, Zn^{2+} is coordinated by three cysteine thiolates (C263, C279 and C343) and one water molecule, which resembles the catalytic

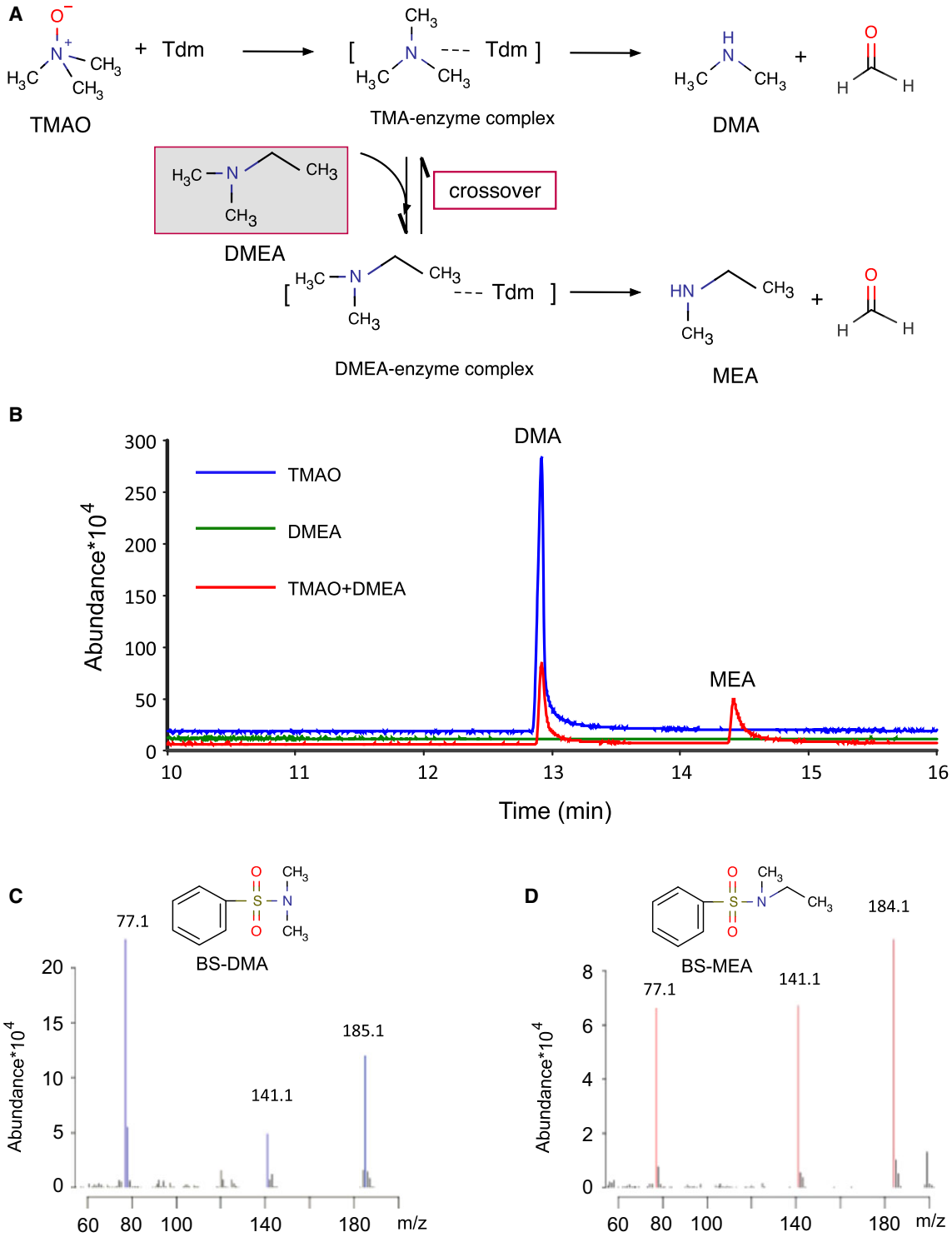

Fig. 4. Formation of a secondary amine product, methylethylamine (MEA) by Tdm using a trimethylamine (TMA) analogue, dimethylethylamine (DMEA). (A) Proposed diagram of MEA formation from DMEA in the presence of the natural substrate trimethylamine *N*-oxide (TMAO). DMA, dimethylamine, HCHO, formaldehyde. (B) Gas chromatography–mass spectrometry (GC-MS) analysis of secondary amines produced during Tdm reaction in the presence or absence of DMEA. The enzyme reaction contains either 50 mM TMAO (blue line), or 25 mM DMEA (green line) or both (red line). Only in the presence of the natural substrate TMAO, MEA was formed (red line). (C) Mass spectra of benzenesulfonyl chloride derivatized secondary amines, BS-DMA (blue) and (D)BS-MEA (red).

Zn^{2+} site of CDA [17–19]. However, caution should be applied when interpreting the Zn^{2+} site in Tdm due to the low quality of the overall model obtained through homology modelling. We cannot rule out the possibility that the fourth Zn^{2+} ligand may be provided by the D198 in Tdm (Fig. 2D).

Indeed, we propose that D198 has a dual role of stabilizing both Zn^{2+} and catalytic Fe^{2+} (Fig. 2C,D). Mutagenesis study of the conserved D198 in Tdm supported that D198 is crucial for maintaining structural integrity through interaction with Zn^{2+}, either directly or indirectly through H-bonding with Zn^{2+}-bound water. Replacing D198 with Ala, Asn and Glu resulted in quaternary structural alteration as well as reduced Zn^{2+} content in the Tdm variants (Table 2).

D198 also likely contributes to Fe^{2+}-binding, together with H276. Results presented in Table 2 demonstrate that a carboxyl group is important in maintaining Fe^{2+} stoichiometry in Tdm and the Fe^{2+}/Tdm ratio of the D198E variant, but not the D198A variant, was comparable to that of the WT. So far, it is unclear what other residue(s) could contribute to Fe^{2+} coordination in Tdm. Tdm may employ a non-classic 2-His-1-carboxylate triad. Variations of the classical 2-His-1-carboxylate triad motif for Fe^{2+} coordination have recently been found in a number of enzymes. For example, in the halogenase SyrB2, the carboxylate is absent and instead, a halogen ion takes its place in the coordination sphere [36]. In diketone-cleaving dioxygenase, Dke1 [37], and cysteine dioxygenase, CDO, a three-histidine triad is found [38,39], whereas in carotenoid oxygenase, a four-histidine motif is present [40,41]. Further structural and biochemical investigations are certainly warranted to conclusively map the ligands involved in Zn^{2+} and Fe^{2+} coordination in Tdm.

Substrate recognition and binding by a hydrophobic pocket

Our site-directed mutagenesis results (F259A, Y305A and W321A) suggest that these residues may contribute to form substrate pocket that recognizes and binds TMAO by cation–π interaction. This interaction has also been found in other TMAO-binding proteins, such as TmoX and TorT [21,22]. The cation–π interaction has long been recognized as an important noncovalent binding interaction relevant to structural biology [23]. The aromatic rings of Phe, Try and Trp provide negative electrostatic potential allowing interaction with cations [42]. Such cation–π interaction also seems common in proteins involved in quaternary amine transport and metabolism, e.g. choline-TMA lyase (CutC) from *Desulfovibrio alaskensis* G20 [43], acetylcholine esterase from *Tetronarce californica* [44,45], substrate-binding protein (ChoX) of choline/acetylcholine from *Sinorhizobium meliloti* [46], and substrate-binding protein (ProX) of glycine betaine from *Archaeoglobus fulgidus* [47]. Interestingly, the Fe^{2+}/Tdm ratios of these variants were also significantly reduced compared to that of the wild-type. It is therefore likely that these hydrophobic residues are located adjacent to the Fe^{2+} centre and thus may directly or indirectly influence Fe^{2+} coordination in Tdm.

The O_2-independent *N*-dealkylation of Tdm

Tdm carries out an oxidative *N*-dealkylation, which resembles other well-characterized α-ketoglutarate-dependent mononuclear non-haem enzymes [24–26]. These α-ketoglutarate-dependent oxygenases activate dioxygen to form high-valent Fe(IV)-oxo species as the oxidant. However, Tdm is different from these oxygenases in that Tdm-catalysed reaction is O_2-independent (Fig. 3A).

Chemically, many single-oxygen atom donors are capable of generating Fe(IV)-oxo species (e.g. NaOX, X = Cl or Br, iodosylbenzene (PhIO)) [48,49]. However, a surrogate single-oxygen atom donor has also been found in biological systems, such as P450 enzymes. *N,N*-dimethylaniline *N*-oxide (DMAO) is an intermediate formed during P450-mediated demethylation of *N,N*-dimethylaniline. Recently, studies have demonstrated that DMAO can serve as a surrogate single-oxygen donor because DMAO gave identical isotope effects as the natural system using NADPH and O_2 [50,51]. We propose that, akin to DMAO for P450 enzymes, TMAO can act as a surrogate oxygen donor for Tdm. A potential mechanism for TMAO degradation catalysed by Tdm is shown in Fig. 3B.

We postulated that a high-valent Fe is responsible for TMAO demethylation (Fig. 3B) and the nature of the active Fe species remains unclear. The Fe(IV)-oxo species is common in haem and non-haem Fe^{2+}-containing enzymes [52–55]. In addition, another high-valent iron-oxo complex, Fe(V)-oxo, has been postulated as an active oxidant in Rieske dioxygenase enzymes [56,57] and authenticated in non-haem iron biomimetic systems [58]. Indeed, our crossover experiments did support the presence of a TMA-alike intermediate during the catalytic cycle as proposed in Fig. 3B. According to this hypothesis, the oxygen atom is transferred from the substrate TMAO to produce formaldehyde via the high-valent iron-oxo intermediate (e.g. Fe(IV)-oxo, Fe(V)-oxo). Clearly further investigations, such as using electron paramagnetic resonance spectroscopy [48,54],

are required to identify the active Fe species involved in Tdm catalysis.

The exact role of Zn^{2+} in the progression of TMAO demethylation also remains unclear. Although our site-directed mutagenesis data largely supported the role of Zn in maintaining Tdm structure, its involvement as a cocatalytic Zn is also possible. For example, one can envisage that Zn^{2+} may facilitate oxygen atom transfer from TMAO to Fe through Lewis acid–base interaction with the O atom at step ② (Fig. 3B). Similarly, Zn^{2+} may bind to the O atom of the complex formed at step ④ to mediate C-N bond cleavage (Fig. 3B). A similar role of Zn in the catalytic site of alcohol dehydrogenase (ADH) for C-H bond cleavage is well known [59]. Alternatively, Zn^{2+} may also stabilize the reactive high-valent Fe-oxo species during catalysis through electrostatic interaction via a solvent oxygen, e.g. Fe(IV)-oxo (step ③, Fig. 3B). It has been shown that the conserved positively charged arginine residue can help to stabilize and polarize the negative charge on the reactive Fe(III)-OOH complex in peroxidase [60–62].

In summary, the combination of site-directed mutagenesis, homology modelling and analytical chemistry have provided insight into the structure–function relationship of a novel Zn^{2+}- and Fe^{2+}-dependent metalloprotein, Tdm. It carries out an unusual O_2-independent oxidative demethylation utilizing the substrate as the oxygen donor. Determination of the three-dimensional structure is now required to validate the model we proposed.

Materials and methods

Cloning, expression and purification of Tdm and variants of *M. silvestris*

Plasmids and strains used for cloning and overexpression of Tdm and its variants in *E. coli* are listed in Tables S1 and S2. Tdm expression and purification were carried out as described previously [3]. Briefly, *E. coli* cells were grown at 37 °C to an OD_{600} of 0.5, and isopropyl β-D-1-thiogalactopyranoside (IPTG) was then added to a final concentration of 0.2 mM. Protein expression was carried out at 18 °C before harvesting. Tdm was purified by 6*His-tag affinity purification from recombinant *E. coli* according to the manufacturer's protocol (Merck, Nottingham, UK). Proteins eluted from the affinity column were further purified by desalting against 20 mM Tris/HCl (pH 7.9), 50 mM NaCl using a HiTrap desalting column (GE Healthcare, Uppsala, Sweden) followed by size-exclusion chromatography using a Superdex 200 10/300 GL column (GE Healthcare). Fractions were pooled and concentrated by ultrafiltration (Amicon Corporation, Danvers, MA, USA). Protein concentrations were determined using a protein assay kit (Bio-Rad, Watford, UK). Site-directed mutations in *tdm* were introduced by PCR and confirmed by DNA sequencing. The oligonucleotides used in this study are shown in the supplementary information.

Enzyme activity assay

Enzyme activity was measured by quantifying HCHO production from TMAO degradation. The reaction mixture for HCHO assays contained 2.5 μg of purified Tdm in 50 μL of 10 mM MES buffer (pH 6.0). The reactions were initiated by adding TMAO (0.6–8 mM final concentration) into the mixture and incubated for 10 min unless otherwise specified [3]. Michaelis–Menten constant (K_m), maximum velocity (V_{max}) and catalytic constant (k_{cat}) were calculated as described previously [3]. Tdm activity was also measured in the absence of oxygen in an anaerobic chamber (MACS-MG-500 anaerobic workstation; Don Whitley Scientific, Shipley, UK). All solutions were degassed prior to use. To test the impact of metal chelators on Tdm activity, a range of concentrations of the following compounds were used, including ethylenediaminetetraacetic acid (EDTA, 0–50 mM), ethylene glycol-bis(β-aminoethyl ether)-*N*,*N*,*N*′,*N*′-tetraacetic acid (EGTA, 0–50 mM) and pyridine-2,6-dicarboxylic acid (PDC, 0–10 mM). Neither PDC nor EGTA affected Tdm activity. Ascorbic acid (0–10 mM) and H_2O_2 (0–100 μM) were also tested in the enzyme assays with 5 mM TMAO to investigate their effects on Tdm activity.

For the metal replacement experiment, purified Tdm was diluted in a buffer containing 20 mM Tris/HCl (pH 7.8) and 50 mM NaCl to a final concentration of 1 $mg{\cdot}mL^{-1}$ and incubated with various metal ions ($MgCl_2$, $MnCl_2$, $Fe(NH_4)_2(SO_4)_2$, $CoCl_2$, $NiSO_4$, $CuSO_4$, $ZnSO_4$) at an M^{2+}/Tdm ratio of 500 for 6 h at 4 °C. Two millimolar ascorbic acid was used when $Fe(NH_4)_2(SO_4)_2$ was applied to maintain Fe^{2+} in its reduced state. About 2.5 μg of Tdm and 5 mM TMAO were used for HCHO assay as described above.

For the Tdm reactivation experiment, the 6*His-tag was removed using thrombin (GE Healthcare, Little Chalfont, UK) according to the manufacturer's instructions. Briefly, 1 mg purified recombinant Tdm was incubated with 10 units of thrombin at 4 °C overnight (16 h). Thrombin and cleaved 6*His-tag were removed by size-exclusion chromatography. Tdm fractions were pooled, and diluted in buffer containing 20 mM Tris/HCl (pH 7.8) and 50 mM NaCl to a final concentration of 1 $mg{\cdot}mL^{-1}$, which was then incubated with 100 μM H_2O_2 for 20 min on ice. Wherever necessary, ascorbic acid and $Fe(NH_4)_2(SO_4)_2$ was added to a final concentration of 500 μM and 10–500 μM respectively. The samples were then incubated for 20 min

on ice prior to the quantification of Tdm activity using the aforementioned HCHO assay.

Fe^{2+} titration

The Fe^{2+} titration (using $Fe(NH_4)_2(SO_4)_2$) was performed with the 6*His-tag-cleaved Tdm. To maintain Fe^{2+} in its reduced form, the titration assay was performed with 2 mM ascorbic acid with varying molar ratios of Fe^{2+}/Tdm in the Tris/NaCl buffer (20 mM Tris, 50 mM NaCl, pH 7.8) for 4 h before HCHO essay was carried out. The titration data for metal stoichiometry (n) determination were analysed by nonlinear curve fitting using Eqn (1) [63,64].

$$y = y_0 + (y_m - y_0) \times \frac{(n + x + K_d) - \sqrt{(n + x + K_d)^2 - 4 \times n \times x}}{2 \times n} \quad (1)$$

where x is the concentration of total metal ion and y is the activity percentage to the maximal activity, y_m is the maximal activity, y_0 is the activity percentage of as-isolated enzyme without added metal, K_d is the dissociation constant and n is the number of binding sites (stoichiometry).

Inductively coupled plasma–mass spectrometry and optical emission spectrometry (ICP-MS/OES)

About 3% (v/v) trace metal grade nitric acid purified in house by sub-boiling point distillation was used as the sample matrix. ICP-MS analyses were carried out on an Agilent Technologies 7500 ICP-MS instrument. ICP-OES was performed on a Perkin Elmer Optical Emission Spectrometer Optima 5300DV instrument. The standards for calibration were freshly prepared by diluting Zn, Fe, S, Ni stock solutions (at 1000 $mg \cdot L^{-1}$; Sigma-Aldrich, Saint Louis, MO, USA) with 3% HNO_3 in doubly deionized water with concentrations from 0.2 to 1 $mg \cdot L^{-1}$ for Zn, Fe and Ni, and from 4 to 20 $mg \cdot L^{-1}$ for S. About 2.4 mg protein was diluted in 3% HNO_3 matrix for metal analysis. The content of S was quantified in order to determine the protein concentration. The contents of Zn, Fe, Ni and S were measured using the emission lines of 213.857 nm (Zn), 234.830 nm (Fe), 231.604 nm (Ni) and 180.669 nm (S) respectively.

Gas chromatography–mass spectrometry (GC-MS) determination of secondary amines

Fifty microgram purified Tdm was incubated at room temperature (~ 20 °C) in a final volume of 1 mL in 10 mM MES buffer (pH 6.0) with either 50 mM TMAO or 25 mM dimethylethylamine (DMEA), or both for 30 min. Secondary amines (i.e. dimethylamine, methylethylamine) were derivatized using benzenesulfonyl chloride (Sigma-Aldrich) and determined by GC-MS as described previously [65].

Homology modelling

A homology model for the DUF1989 domain of Tdm (residues 1–383) was created using the DUF1989 domain family protein (PDB: 3ORU) as the template using the SWISS-MODEL webserver (http://swissmodel.expasy.org) [66]. Three-dimensional structures were visualized using chimera [67].

Secondary and quaternary structure determination

Secondary structure was determined by circular dichroism using a Jasco J-815 spectrometer (Jasco, Great Dunmow, UK) and the secondary structure components (α-helix, β-sheet, turn and random coil) were estimated using the CDSSTR algorithm with reference set 7 from the DICHROWEB website as described previously [68,69]. Quaternary structure was determined by size-exclusion chromatography on a Superdex 200 10/300 GL gel filtration column (GE Healthcare, Uppsala, Sweden) equilibrated with buffer containing 20 mM Tris/HCl (pH 7.8) and 100 mM NaCl at 0.7 $mL \cdot min^{-1}$ using an AKTA FPLC system (GE Healthcare, Chalfont St. Giles, UK).

Multiple sequence alignments

Multiple sequence alignments were performed using the iterative alignment program MUSCLE [70].

Statistical analyses

Analysis of variance (ANOVA) and Tukey HSD *post hoc* tests were performed using the R software package version 3.2.1 [71]. Data are expressed as means ± SD.

Acknowledgements

We acknowledge a joint Warwick Chancellors International Scholarship and MIBTP for funding (YZ). This work is partially supported by the Natural Environment Research Council (NE/M002233).

Author contributions

YZ, HS, TDHB, CAB and YC planned and designed research. YZ and AZK performed research. YZ, AZK, HS, TDHB, CAB and YC analysed the data and wrote the paper.

Conflict of interest

The authors declare no conflict of interest.

References

1 Chen Y, Patel NA, Crombie A, Scrivens JH & Murrell JC (2011) Bacterial flavin-containing monooxygenase is trimethylamine monooxygenase. *Proc Natl Acad Sci USA* **108**, 17791–17796.

2 Lidbury I, Murrell JC & Chen Y (2014) Trimethylamine *N*-oxide metabolism by abundant marine heterotrophic bacteria. *Proc Natl Acad Sci USA* **111**, 2710–2715.

3 Zhu Y, Jameson E, Parslow RA, Lidbury I, Fu T, Dafforn TR, Schäfer H & Chen Y (2014) Identification and characterization of trimethylamine *N*-oxide (TMAO) demethylase and TMAO permease in *Methylocella silvestris* BL2. *Environ Microbiol* **16**, 3318–3330.

4 Myers PA & Zatman LJ (1971) The metabolism of trimethylamine *N*-oxide by *Bacillus* PM6. *Biochem J* **121**, 10P.

5 Large PJ (1971) Non-oxidative demethylation of trimethylamine *N*-oxide by *Pseudomonas aminovorans*. *FEBS Lett* **18**, 297–300.

6 Kanamori T, Kanou N, Atomi H & Imanaka T (2004) Enzymatic characterization of a prokaryotic urea carboxylase. *J Bacteriol* **186**, 2532–2539.

7 Okamura-Ikeda K, Hosaka H, Yoshimura M, Yamashita E, Toma S, Nakagawa A, Fujiwara K, Motokawa Y & Taniguchi H (2005) Crystal structure of human T-protein of glycine cleavage system at 2.0 Å resolution and its implication for understanding non-ketotic hyperglycinemia. *J Mol Biol* **351**, 1146–1159.

8 Schuller DJ, Reisch CR, Moran MA, Whitman WB & Lanzilotta WN (2012) Structures of dimethylsulfoniopropionate-dependent demethylase from the marine organism *Pelagabacter ubique*. *Protein Sci* **21**, 289–298.

9 Gantt SL, Gattis SG & Fierke CA (2006) Catalytic activity and inhibition of human histone deacetylase 8 is dependent on the identity of the active site metal ion. *Biochemistry* **45**, 6170–6178.

10 Zhu J, Dizin E, Hu X, Wavreille AS, Park J & Pei D (2003) S-Ribosylhomocysteinase (LuxS) is a mononuclear iron protein. *Biochemistry* **42**, 4717–4726.

11 Latypova E, Yang S, Wang YS, Wang T, Chavkin TA, Hackett M, Schäfer H & Kalyuzhnaya MG (2010) Genetics of the glutamate-mediated methylamine utilization pathway in the facultative methylotrophic beta-proteobacterium *Methyloversatilis universalis* FAM5. *Mol Microbiol* **75**, 426–439.

12 Benkert P, Biasini M & Schwede T (2011) Toward the estimation of the absolute quality of individual protein structure models. *Bioinformatics* **27**, 343–350.

13 Hegg EL & Que L (1997) The 2-His-1-carboxylate facial triad – an emerging structural motif in mononuclear non-heme iron(II) enzymes. *Eur J Biochem* **250**, 625–629.

14 Koehntop KD, Emerson JP & Que L (2005) The 2-His-1-carboxylate facial triad: a versatile platform for dioxygen activation by mononuclear non-heme iron(II) enzymes. *J Biol Inorg Chem* **10**, 87–93.

15 Auld DS (2001) Zinc coordination sphere in biochemical zinc sites. *Biometals* **14**, 271–313.

16 Harding MM (2001) Geometry of metal-ligand interactions in proteins. *Acta Crystallogr D Biol Crystallogr* **57**, 401–411.

17 Sánchez-Quitian ZA, Schneider CZ, Ducati RG, de Azevedo WF, Bloch C, Basso LA & Santos DS (2010) Structural and functional analyses of *Mycobacterium tuberculosis* Rv3315c-encoded metal-dependent homotetrameric cytidine deaminase. *J Struct Biol* **169**, 413–423.

18 Chung SJ, Fromme JC & Verdine GL (2005) Structure of human cytidine deaminase bound to a potent inhibitor. *J Med Chem* **48**, 658–660.

19 Teh AH, Kimura M, Yamamoto M, Tanaka N, Yamaguchi I & Kumasaka T (2006) The 1.48 Å resolution crystal structure of the homotetrameric cytidine deaminase from mouse. *Biochemistry* **45**, 7825–7833.

20 Kumasaka T, Yamamoto M, Furuichi M, Nakasako M, Teh AH, Kimura M, Yamaguchi I & Ueki T (2007) Crystal structures of blasticidin S deaminase (BSD): implications for dynamic properties of catalytic zinc. *J Biol Chem* **282**, 37103–37111.

21 Li CY, Chen XL, Shao X, Wei TD, Wang P, Xie BB, Qin QL, Zhang XY, Su HN, Song XY *et al.* (2015) Mechanistic insight into trimethylamine *N*-oxide recognition by the marine bacterium *Ruegeria pomeroyi* DSS-3. *J Bacteriol* **197**, 3378–3387.

22 Moore JO & Hendrickson WA (2012) An asymmetry-to-symmetry switch in signal transmission by the histidine kinase receptor for TMAO. *Structure* **20**, 729–741.

23 Gallivan JP & Dougherty DA (1999) Cation-pi interactions in structural biology. *Proc Natl Acad Sci USA* **96**, 9459–9464.

24 Mishina Y & He C (2006) Oxidative dealkylation DNA repair mediated by the mononuclear non-heme iron AlkB proteins. *J Inorg Biochem* **100**, 670–678.

25 Tsukada Y, Fang J, Erdjument-Bromage H, Warren ME, Borchers CH, Tempst P & Zhang Y (2006) Histone demethylation by a family of JmjC domain-containing proteins. *Nature* **439**, 811–816.

26 Chang B, Chen Y, Zhao Y & Bruick RK (2007) JMJD6 is a histone arginine demethylase. *Science* **318**, 444–447.

27 Daughtry KD, Xiao Y, Stoner-Ma D, Cho E, Orville AM, Liu P & Allen KN (2012) Quaternary ammonium

oxidative demethylation: X-ray crystallographic, resonance raman, and UV-visible spectroscopic analysis of a Rieske-type demethylase. *J Am Chem Soc* **134**, 2823–2834.
28 Summers RM, Louie TM, Yu CL, Gakhar L, Louie KC & Subramanian M (2012) Novel, highly specific *N*-demethylases enable bacteria to live on caffeine and related purine alkaloids. *J Bacteriol* **194**, 2041–2049.
29 Hrycay EG & Bandiera SM (2015) Monooxygenase, peroxidase and peroxygenase properties and reaction mechanisms of cytochrome P450 enzymes. *Adv Exp Med Biol* **851**, 1–61.
30 Guengerich FP, Yun CH & Macdonald TL (1996) Evidence for a 1-electron oxidation mechanism in N-dealkylation of N, N-dialkylanilines by cytochrome P450 2B1. Kinetic hydrogen isotope effects, linear free energy relationships, comparisons with horseradish peroxidase, and studies with oxygen surrogates. *J Biol Chem* **271**, 27321–27329.
31 Back TG & Dyck BP (1997) A novel camphor-derived selenenamide that acts as a glutathione peroxidase mimetic. *J Am Chem Soc* **119**, 2079–2083.
32 Daumann LJ, McCarthy BY, Hadler KS, Murray TP, Gahan LR, Larrabee JA, Ollis DL & Schenk G (2013) Promiscuity comes at a price: catalytic versatility vs efficiency in different metal ion derivatives of the potential bioremediator GpdQ. *Biochim Biophys Acta* **1834**, 425–432.
33 Zang TM, Hollman DA, Crawford PA, Crowder MW & Makaroff CA (2001) Arabidopsis glyoxalase II contains a zinc/iron binuclear metal center that is essential for substrate binding and catalysis. *J Biol Chem* **276**, 4788–4795.
34 Kress D, Alhapel A, Pierik AJ & Essen LO (2008) The crystal structure of enamidase: a bifunctional enzyme of the nicotinate catabolism. *J Mol Biol* **384**, 837–847.
35 Namgaladze D, Hofer HW & Ullrich V (2002) Redox control of calcineurin by targeting the binuclear Fe^{2+}-Zn^{2+} center at the enzyme active site. *J Biol Chem* **277**, 5962–5969.
36 Blasiak LC, Vaillancourt FH, Walsh CT & Drennan CL (2006) Crystal structure of the non-haem iron halogenase SyrB2 in syringomycin biosynthesis. *Nature* **440**, 368–371.
37 Diebold AR, Neidig ML, Moran GR, Straganz GD & Solomon EI (2010) The three-his triad in Dke1: comparisons to the classical facial triad. *Biochemistry* **49**, 6945–6952.
38 McCoy JG, Bailey LJ, Bitto E, Bingman CA, Aceti DJ, Fox BG & Phillips GN (2006) Structure and mechanism of mouse cysteine dioxygenase. *Proc Natl Acad Sci USA* **103**, 3084–3089.
39 Gardner JD, Pierce BS, Fox BG & Brunold TC (2010) Spectroscopic and computational characterization of substrate-bound mouse cysteine dioxygenase: nature of the ferrous and ferric cysteine adducts and mechanistic implications. *Biochemistry* **49**, 6033–6041.
40 Kloer DP, Ruch S, Al-Babili S, Beyer P & Schulz GE (2005) The structure of a retinal-forming carotenoid oxygenase. *Science* **308**, 267–269.
41 Poliakov E, Gentleman S, Cunningham FX Jr, Miller-Ihli NJ & Redmond TM (2005) Key role of conserved histidines in recombinant mouse β-Carotene 15,15′-monooxygenase-1 activity. *J Biol Chem* **280**, 29217–29223.
42 Dougherty DA (1996) Cation-pi interactions in chemistry and biology: a new view of benzene, Phe, Tyr, and Trp. *Science* **271**, 163–168.
43 Craciun S, Marks JA & Balskus EP (2014) Characterization of choline trimethylamine-lyase expands the chemistry of glycyl radical enzymes. *ACS Chem Biol* **9**, 1408–1413.
44 Zhong W, Gallivan JP, Zhang Y, Li L, Lester HA & Dougherty DA (1998) From *ab initio* quantum mechanics to molecular neurobiology: a cation-pi binding site in the nicotinic receptor. *Proc Natl Acad Sci USA* **95**, 12088–12093.
45 Harel M, Schalk I, Ehret-Sabatier L, Bouet F, Goeldner M, Hirth C, Axelsen PH, Silman I & Sussman JL (1993) Quaternary ligand binding to romatic residues in the active-site gorge of acetylcholinesterase. *Proc Natl Acad Sci USA* **90**, 9031–9035.
46 Oswald C, Smits SH, Höing M, Sohn-Bösser L, Dupont L, Le Rudulier D, Schmitt L & Bremer E (2008) Crystal structures of the choline/acetylcholine substrate-binding protein ChoX from *Sinorhizobium meliloti* in the liganded and unliganded-closed states. *J Biol Chem* **283**, 32848–32859.
47 Schiefner A, Holtmann G, Diederichs K, Welte W & Bremer E (2004) Structural basis for the binding of compatible solutes by ProX from the hyperthermophilic archaeon *Archaeoglobus fulgidus*. *J Biol Chem* **279**, 48270–48281.
48 Rohde JU, In JH, Lim MH, Brennessel WW, Bukowski MR, Stubna A, Münck E, Nam W & Que L (2003) Crystallographic and spectroscopic characterization of a nonheme Fe(IV)-O complex. *Science* **299**, 1037–1039.
49 Balland V, Charlot M, Banse F, Girerd J, Mattioli T, Bill E, Bartoli J, Battioni P & Mansuy D (2004) Spectroscopic characterization of an Fe-IV intermediate generated by reaction of XO^- (X = Cl, Br) with an Fe-II complex bearing a pentadentate non-porphyrinic ligand – hydroxylation and epoxidation activity. *Eur J Inorg Chem* **2**, 301–308.
50 Roberts KM & Jones JP (2010) Anilinic *N*-oxides support cytochrome P450-mediated *N*-dealkylation through hydrogen-atom transfer. *Chemistry* **16**, 8096–8107.

51 Dowers TS, Rock DA & Jones JP (2004) Kinetic isotope effects implicate the iron-oxene as the sole oxidant in P450-catalyzed *N*-dealkylation. *J Am Chem Soc* **126**, 8868–8869.
52 Makris TM, von Koenig K, Schlichting I & Sligar SG (2006) The status of high-valent metal oxo complexes in the P450 cytochromes. *J Inorg Biochem* **100**, 507–518.
53 Costas M, Mehn MP, Jensen MP & Que L (2004) Dioxygen activation at mononuclear nonheme iron active sites: enzymes, models, and intermediates. *Chem Rev* **104**, 939–986.
54 Krebs C, Galonić Fujimori D, Walsh CT & Bollinger JM (2007) Non-heme Fe(IV)-oxo intermediates. *Acc Chem Res* **40**, 484–492.
55 Nehru K, Seo MS, Kim J & Nam W (2007) Oxidative *N*-dealkylation reactions by oxoiron(IV) complexes of nonheme and heme ligands. *Inorg Chem* **46**, 293–298.
56 Shan X & Que L (2006) High-valent nonheme iron-oxo species in biomimetic oxidations. *J Inorg Biochem* **100**, 421–433.
57 Kovaleva EG & Lipscomb JD (2008) Versatility of biological non-heme Fe(II) centers in oxygen activation reactions. *Nat Chem Biol* **4**, 186–193.
58 Tiago de Oliveira F, Chanda A, Banerjee D, Shan X, Mondal S, Que L, Bominaar EL, Münck E & Collins TJ (2007) Chemical and spectroscopic evidence for an Fe(V)-oxo complex. *Science* **315**, 835–838.
59 Bugg T (2012) *Introduction to Enzyme and Coenzyme Chemistry*, 3rd edn. Wiley, Chichester, UK.
60 Schiødt CB, Veitch NC & Welinder KG (2007) Roles of distal arginine in activity and stability of *Coprinus cinereus* peroxidase elucidated by kinetic and NMR analysis of the Arg51Gln, -Asn, -Leu, and -Lys mutants. *J Inorg Biochem* **101**, 336–347.
61 Neri F, Indiani C, Welinder KG & Smulevich G (1998) Mutation of the distal arginine in *Coprinus cinereus* peroxidase – structural implications. *Eur J Biochem* **251**, 830–838.
62 Singh R, Grigg JC, Armstrong Z, Murphy ME & Eltis LD (2012) Distal heme pocket residues of B-type dye-decolorizing peroxidase: arginine but not aspartate is essential for peroxidase activity. *J Biol Chem* **287**, 10623–10630.
63 Drake AW & Klakamp SL (2007) A rigorous multiple independent binding site model for determining cell-based equilibrium dissociation constants. *J Immunol Methods* **318**, 147–152.
64 Chai SC, Lu JP & Ye QZ (2009) Determination of binding affinity of metal cofactor to the active site of methionine aminopeptidase based on quantitation of functional enzyme. *Anal Biochem* **395**, 263–264.
65 Zhang H, Ren S, Yu J & Yang M (2012) Occurrence of selected aliphatic amines in source water of major cities in China. *J Environ Sci (China)* **24**, 1885–1890.
66 Arnold K, Bordoli L, Kopp J & Schwede T (2006) The SWISS-MODEL workspace: a web-based environment for protein structure homology modelling. *Bioinformatics* **22**, 195–201.
67 Pettersen EF, Goddard TD, Huang CC, Couch GS, Greenblatt DM, Meng EC & Ferrin TE (2004) UCSF Chimera – a visualization system for exploratory research and analysis. *J Comput Chem* **25**, 1605–1612.
68 Sreerama N & Woody RW (2000) Estimation of protein secondary structure from CD spectra: comparison of CONTIN, SELCON and CDSSTR methods with an expanded reference set. *Anal Biochem* **287**, 252–260.
69 Whitmore L & Wallace BA (2008) Protein secondary structure analyses from circular dichroism spectroscopy: methods and reference databases. *Biopolymers* **89**, 392–400.
70 Edgar R (2004) MUSCLE: multiple sequence alignment with high accuracy and high throughput. *Nucleic Acids Res* **32**, 1792–1797.
71 R Core Team (2015) R: a language and environment for statistical computing. R Foundation for Statistical Computing, Vienna, Austria.

Supporting information

Additional Supporting Information may be found online in the supporting information tab for this article:

Table S1. Bacterial strains and plasmids used in this study.

Table S2. Primers used for site-directed mutagenesis of Tdm.